Journal of Materials Science: Materials in Electronics (2019) 30:10224–10232
https://doi.org/10.1007/s10854-019-01359-0

Experimental and quantum chemical investigation on imidazolium trifluoroacetate single crystal for optoelectronic applications

Radhakrishnan Anbarasan[1] · **Jeyaperumal Kalyana Sundar**[1]

Received: 8 March 2019 / Accepted: 16 April 2019 / Published online: 2 May 2019

Abstract
The nonlinear optical single crystal of imidazolium trifluoroacetate (ITF) was grown by the solvent evaporation technique. The crystal is subjected to various experimental characterizations such as X-ray diffraction, vibrational, optical, thermal and NLO analysis. In parallel, the molecular functional properties are explored by density functional theory. The inter and intramolecular charge transfer interactions stabilization energies are assessed from the NBO analysis. The material has more than 60% transmission in the entire visible region, and the melting point of the crystal is 143 °C. The HOMO–LUMO energy gaps and the molecular charge transfer properties are investigated by frontier molecular orbital analysis. The existence of intermolecular interactions in the crystal was quantitatively interpreted from the Hirshfeld surface analysis. The ITF crystal possesses 1.67 higher second harmonic generation efficiency compared to typical KDP material.

1 Introduction

The development of new nonlinear optical materials is very emerging field in the last two decades, because of their vast applications in laser optics, optical communication, moderator systems, etc. [1–3]. Second harmonic generation is a well-recognized process for higher-order nonlinear optical progression. Researchers always focus on new efficient material with essential properties. Inorganic materials hold a strong position on nonlinear optical materials on account of high laser damage threshold, good mechanical strength, and high melting point. Organic NLO materials have distinctive physicochemical properties such as the higher order of nonlinear efficiency and good structural flexibility. The strong donor to acceptor electronic transition in delocalized electrons greatly enhanced the nonlinearity of the material.

Nevertheless, it has a lower laser damage threshold, mechanical strength, and melting point. In the case of semi-organic materials, they possess integrated properties of organic and inorganic compounds resembling high melting point, more nonlinear efficiency, mechanical strength, and high laser damage threshold [3–7]. Azole derivatives materials take an assertive role in industrial and pharmacological fields. Imidazole is the decisive materials from azole derivative and its mostly used in sensing, drug design, and optical applications. In literature, the researchers have already reported numerous imidazole derivatives for NLO application such as imidazolium tetrafluoroborate, imidazolium picrate, and imidazolium tartrate, etc., [8–11]. Moreover, the effect of delocalized electrons around the imidazolium ring extensively increase the nonlinearity of the materials, and the effect of strong hydrogen bonds with anions are formulating the crystal packing stability of the material.

In this work, we have grown the novel nonlinear optical material, imidazolium trifluoroacetate (ITF) by a slow evaporation method. Besides, physicochemical properties investigated by a combined way of experimental results with quantum chemical calculations such as X-ray diffraction, vibrational, optical, thermal analysis, frontier molecular orbital analysis, NLO analysis and Hirshfeld surface analysis.

2 Materials and methods

2.1 Synthesis procedure

All the chemicals used in the synthesis are purchased from Merck and used without further purifications. The title compound was synthesized, and the crystal was grown by the slow evaporation method. Initially, equimolar amounts

✉ Jeyaperumal Kalyana Sundar
jksundar50@gmail.com

[1] Department of Physics, Materials Science Laboratory, Periyar University, Salem, Tamil Nadu, 636 011, India

of imidazole and trifluoroacetic acid are used to make the solution. The saturated solution was obtained for under continuous stirring for 6 h at room temperature. The saturated solution was transferred to petri-dish, after 20 days of slow evaporation, a well transparent colorless crystal was obtained as displayed in Fig. 1. The size of the crystal is about $4 \times 4 \times 1$ mm^3.

2.2 Computational details

The structural accompanying molecular properties are extensively explored through quantum chemical calculations. All the theoretical calculations are implemented with the Gaussian 09W program, and their results are visualized with GaussView 5.0 software [12–14]. The initialization of geometry was readily obtained from crystallographic information data, and the structure was optimized without any constraint on the geometry. The ITF molecule was optimized at the B3LYP method, and 6–31 G(d, p) basis set in density functional theory. The nonexistence of negative vibrational frequencies validates energy of the optimized geometry as local minima. The natural bond orbital (NBO) analysis and frontier molecular orbitals calculations are carried out with density functional theory. The polarizabilities, first-order polarizability tensor components, and total first-order polarizability values are calculated from the finite field method. The optimized geometry of ITF was shown in Fig. 2. The calculated optimized structural parameters have resembled with X-ray diffraction data and as depicted in the Table 1. The calculated structural parameters decently agree with X-ray diffraction bond length and angles [15]. The bond length variation in N5–H6 is due to the effect of the strong intermolecular interaction with electronegative atom O13. The smallest structural parameter's variations are due to the nonexistence of crystal packing effects in the optimized gas phase geometry in the optimization process.

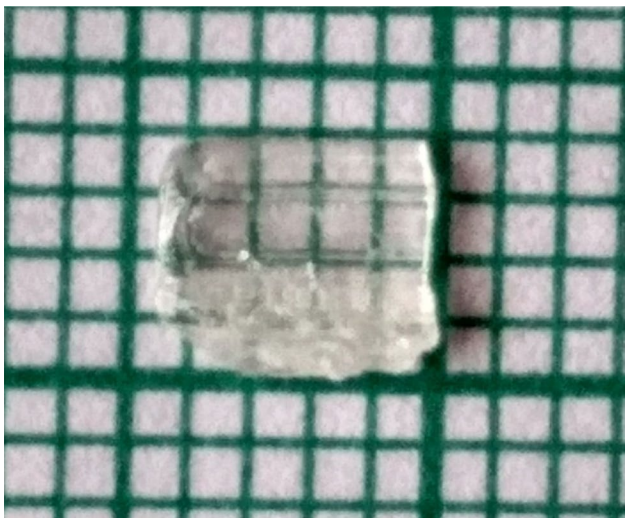

Fig. 1 Photograph of as grown crystal

3 Results and Discussion

3.1 X-ray diffraction analysis

The structural analysis was carried out by powder X-ray diffraction analysis utilizing Rigaku MiniFlex diffractometer in the two-theta angle of 5°–70°. The plane values (hkl) are calculated using Treor program [16] and indexed for the two theta angles in Fig. 3. As seen from the compared XRD pattern, the experimental powder XRD pattern has precisely matched with the simulated XRD pattern of ITF from Mercury program, and it validated the grown crystal structure was identical with previously reported [15]. The lattice parameters are calculated from the powder XRD pattern using unit cell win program. The calculated lattice

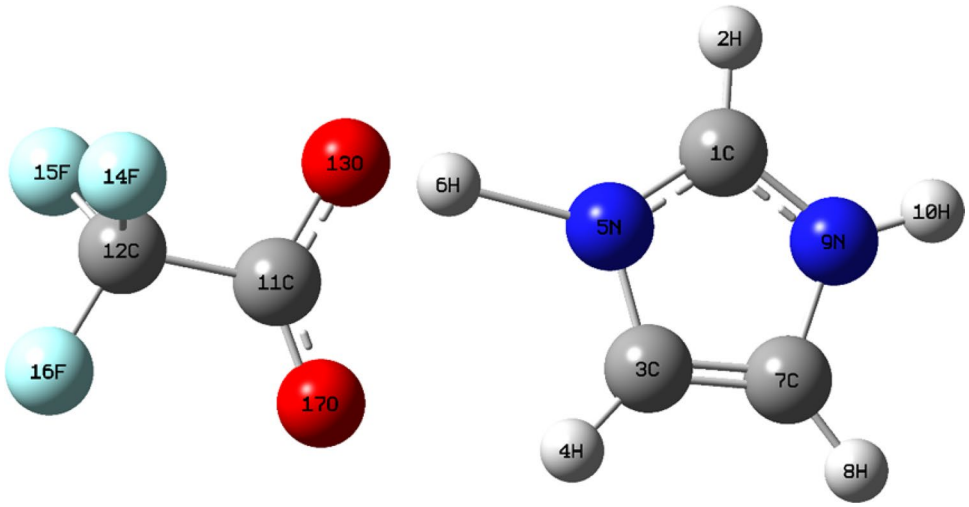

Fig. 2 Optimized geometry of ITF

Table 1 The optimized structural bond lengths, bond angles compared with experimental data

	X-ray diffraction [15]	DFT
Bond length (Å)		
C1–H2	0.9498	1.0800
C1–N9	1.3159	1.3584
C1–N5	1.3159	1.3188
C3–H4	0.9499	1.0796
C3–C7	1.3563	1.3688
C3–N5	1.3454	1.3796
C7–H8	0.9499	1.0781
C7–N9	1.3454	1.3819
N5–H6	0.8799	1.6232
N9–H10	0.8799	1.0085
C11–O13	1.2235	1.3138
C11–O17	1.2236	1.2136
C11–C12	1.5260	1.5463
C12–F14	1.4843	1.3481
C12—F15	1.3072	1.3472
C12–F16	1.2727	1.3376
Angles (°)		
C1–N5–C3	107.912	106.537
C1–N9–C7	107.908	107.778
N5–C3–C7	107.214	109.583
N9–C7–C3	107.214	105.511
O13–C11–O17	129.411	128.054
O13–C11–C12	115.295	110.556
O17–C11–C12	115.294	121.389
C11–C12–F14	101.546	110.397
C11–C12–F15	114.466	110.796
C11–C12–F16	117.918	110.938

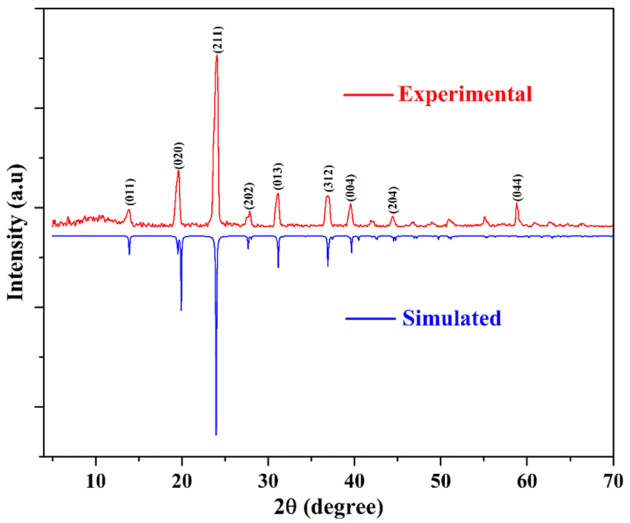

Fig. 3 Powder X-ray diffraction pattern of ITF

Table 2 Lattice parameters comparison of ITF

	Lattice parameters	Crystal system & space group
Present work (ITF)	a = 9.118 Å, b = 8.906 Å, c = 9.142 Å, α = β = υ = 90°, V = 742.608 Å^3	Orthorhombic & $I2_12_12_1$
Reported [15]	a = 9.139 Å, b = 8.906 Å, c = 9.083 Å, α = β = υ = 90°, V = 739.382 Å^3	Orthorhombic & $I2_12_12_1$

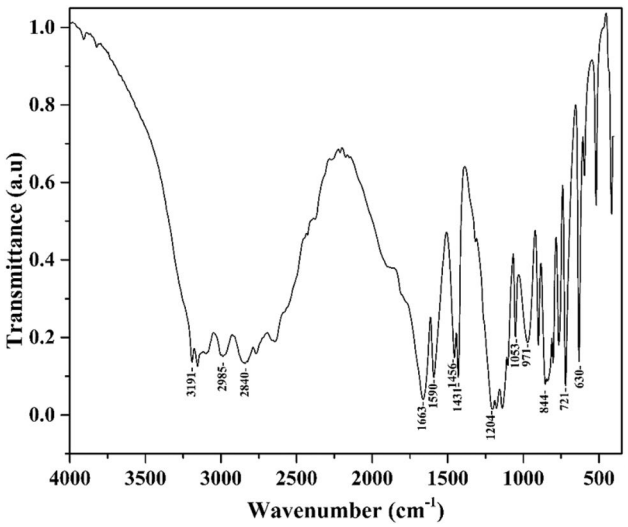

Fig. 4 FTIR spectra of ITF

parameters are adequately matched with previous work and were displayed in Table 2.

3.2 Vibrational analysis

The functional groups present in the titled compound confirmed by vibrational analysis, and corresponding spectra was depicted in Fig. 4. The characteristic and protonation stretching vibrations of imidazolium NH are observed at 3191 cm^{-1} and 2840 cm^{-1}. The stretching mode of CH vibration was interpreted at 2985 cm^{-1}. The anionic COO^- characteristic asymmetric and symmetric stretching vibration is observed at 1663 cm^{-1} and 1590 cm^{-1} respectively. The sharp absorption peak at 1456 cm^{-1} and 1431 cm^{-1} are corresponding to the asymmetric and symmetric stretching vibrations of CF_3. The peaks around 1204 cm^{-1}–1101 cm^{-1} are attributed to the COO^- bending and C–C stretching vibrations of trifluoroacetate anion. The peaks within the range of 1053–900 cm^{-1} are corresponding to the C–C–O and C–C–F bending vibration of trifluoroacetate. The lower range absorption peaks around

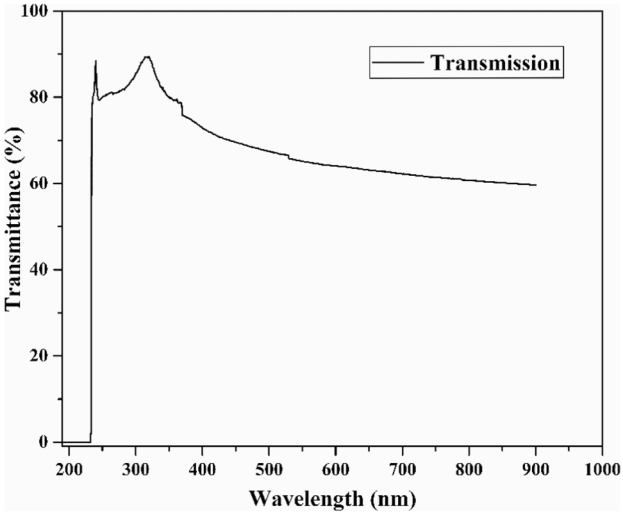

Fig. 5 Transmission spectra of ITF

721 cm^{-1} and 630 cm^{-1} depicts the ring deformation of imidazolium moiety.

3.3 Optical analysis

Optical transparency and an optical window region of the material is the deciding factors for optical applications. The optical properties were investigated by Perkin Elmer UV–Vis NIR spectrometer in the wavelength range of 190–900 nm. The Fig. 5 displays the transmission spectra of ITF, and the transmission is starting from 233 nm. The material secured 60% transmission in the entire visible region and an optical window of ITF is 233–900 nm. The lower cut-off wavelength of the material is 233 nm, and the representing band gap value is 5.32 eV. The moderate transmission in the whole visible region reveals that ITF crystal is suitable for optoelectronic application in the entire visible region.

3.4 Natural bond orbital (NBO) analysis

The inter, intramolecular and hybridizations of electrons were effectively calculated from the NBO analysis. It is calculated from the function of DFT/B3LYP using NBO 3.1 program implemented with the Gaussian 09W package in order to understand the electron transition from bonding orbital to virtual orbitals [18–20]. All the orbitals in the molecules were mathematically constituted and described the electron density of the molecules in the way of second-order perturbation theory. The strengths of the inter and intramolecular and hydrogen bond interactions were mathematically calculated from second-order perturbation energy, where q_i is the donor orbital occupancy, $F_{(i,j)}$ is the second order Fock matrix elements and ε_i and ε_j are the diagonal elements.

$$E^{(2)} = \Delta E_{i,j} = q_i \left(\frac{F^2_{(i,j)}}{\varepsilon_j - \varepsilon_i} \right)$$

The imidazolium trifluoroacetate was strongly interconnected with hydrogen bond N5–H6···O13; presumably, it has high stabilization energy 49.85 kcal/mol. In azole ring due to the impact of intramolecular delocalization electrons in the molecule, C1–N5 and C3–C7 have high stabilization energies of 19.88 kcal/mol and 15.17 kcal/mol respectively. The lone pair electrons of N and O intensely interact with ITF molecule through inter and intramolecular interactions. The stabilization energies associated with these interactions N9 (n1) → C1–N5(π*) and N9 (n1) → C3–C7(π*) are assessed about 53.68 and 29.24 kcal/mol confirm the nitrogen lone pair electrons delocalize over the azole ring. The leading stabilization energy in the ITF molecule is 63.63 kcal/mol is corresponding to the transition O13 (n2) → C11–O17(π*). The lone pair electron transition of fluorine atoms has the least interaction energy compared to N and O, which are presented in Table 3.

3.5 Frontier molecular orbital analysis (FMO)

The charge transfers mechanism, chemical reactivity, and their reaction paths are illustrated from the frontier molecular orbital analysis [19, 21–23]. In FMO, the two orbitals are the most effective which are the highest occupied molecular orbital (HOMO) and lowest unoccupied molecular orbital (LUMO). The HOMO is mostly localized over the donor site of the molecule likely LUMO is localized over the acceptor site of a molecule. The frontier molecular orbitals and energy gap of ITF is shown in Fig. 6. HOMO is mostly localized on the imidazolium site of ITF, and LUMO is localized over the entire molecule of ITF. The HOMO molecular orbital shape indicating the bonding molecular orbitals (π) and the shape of LUMO orbitals indicating the antibonding molecular orbitals (π*). The calculated HOMO value is − 6.968 eV, LUMO value is − 0.044 eV, and their energy gap is 6.968 eV. The global chemical reactivity descriptors are explored the chemical reactivity, biological activity and reactions site of the molecule. From the Koopman's theorem, the chemical potential (μ), global hardness (η), electronegativity (χ), softness (ζ) and electrophilic index (ω) were calculated, and the values are listed in Table 4 [23]. According to softness-hardness rule, a molecule having lower softness value is less reactive and wider energy gap pointed the higher thermal and chemical stability of the molecule. The lower softness value of the ITF molecule reveals that the title compound is under hard molecule category and the higher HOMO–LUMO energy gap indicated

Table 3 Second-order perturbation theory analysis of fock matrix in NBO basis

Donor (i)	Acceptor (j)	E(2) kcal/mol	E(j)–E(i) a.u	F(i,j) a.u	Type
BD (2) C1–N5	BD*(2) C3–C7	19.88	0.35	0.077	π–π*
BD (2) C3–C7	BD*(2) C1–N5	15.17	0.26	0.06	π–π*
LP (1) N5	BD*(1) C1–N9	7.26	0.84	0.072	n–π*
LP (1) N5	BD*(1) C3–C7	4.42	0.98	0.061	n–π*
LP (1) N9	BD*(2) C1–N5	53.68	0.27	0.108	n–π*
LP (1) N9	BD*(2) C3–C7	29.24	0.31	0.088	n–π*
LP (1) N5	BD*(1) H6–O13	49.85	0.79	0.179	n–σ*
LP (1) O13	BD*(1) C11–O17	10.79	1.16	0.100	n–π*
LP (2) O13	BD*(2) C11–O17	63.63	0.31	0.127	n–π*
LP (2) F14	BD*(1) C11–C12	7.25	0.72	0.066	n–σ*
LP (3) F14	BD*(1) C12–F15	13.37	0.65	0.084	n–σ*
LP (3) F15	BD*(1) C12–F14	13.43	0.65	0.084	n–σ*
LP (3) F16	BD*(1) C12–F14	12.16	0.65	0.080	n–σ*
LP (3) F16	BD*(1) C12–F15	11.91	0.65	0.080	n–σ*
LP (2) O17	BD*(1) C11–C12	25.77	0.56	0.108	n–σ*
LP (2) O17	BD*(1) C11–O13	27.25	0.69	0.124	n–σ*

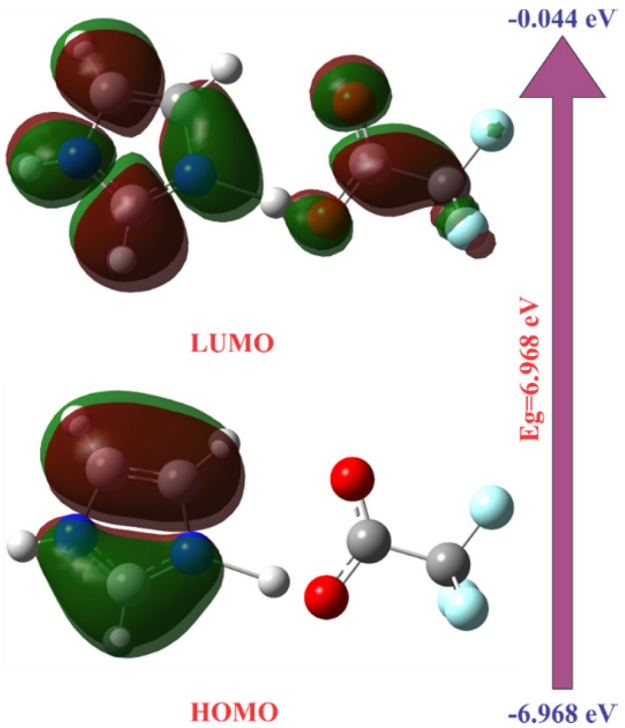

Fig. 6 Frontier molecular orbitals of ITF

the intermolecular charge transfer between the cation and anions. From these results, the delocalization electrons of the imidazolium ring enhance the nonlinear optical activity of ITF molecule.

Table 4 Frontier molecular energies and global chemical reactivity values of ITF

Parameters	Calculated values (eV)
HOMO energy	−6.968
LUMO energy	−0.044
HOMO–LUMO energy gap	6.924
Ionization potential (IP = − HOMO)	6.968
Electron affinity (IA = − LUMO)	0.044
Electronegativity $\left(\chi = \frac{(IP+IA)}{2}\right)$	3.506
Chemical potential ($\mu = -\chi$)	−3.506
Global hardness $\left(\eta = \frac{(IP-IA)}{2}\right)$	3.462
Softness $\left(\zeta = \frac{1}{2\eta}\right)$	0.144
Electrophilic index $\left(\omega = \frac{\mu^2}{2\eta}\right)$	1.775

3.6 Thermal analysis

Thermal stability of the ITF crystal was appropriately investigated by simultaneous thermogravimetric, and differential thermal analysis using TA SDT Q600 V20.9 build 20, in the temperature range of 29–348 °C at a heating rate of 10 °C/min in a nitrogen atmosphere. The material has a two-stage decomposition, and it is initialized at 142 °C. As seen from Fig. 7. The two sharp endothermic peaks are observed at 142 °C and 250 °C, and they are corresponding to the decomposition points of azole ring and trifluoroacetate anion. The first endothermic peak at 142 °C indicates the melting point of the ITF crystal. There is no

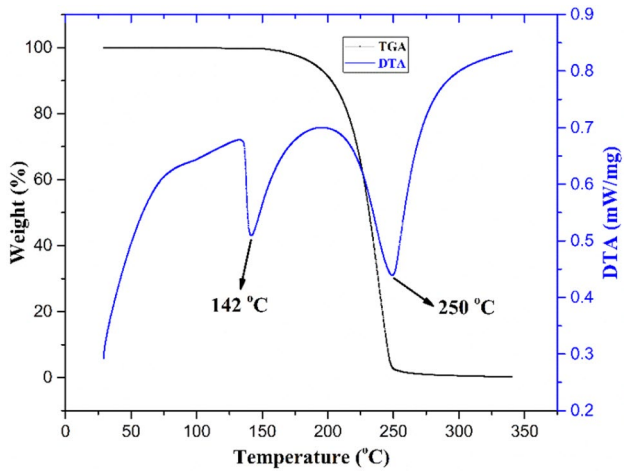

Fig. 7 TG/DTA plot of ITF

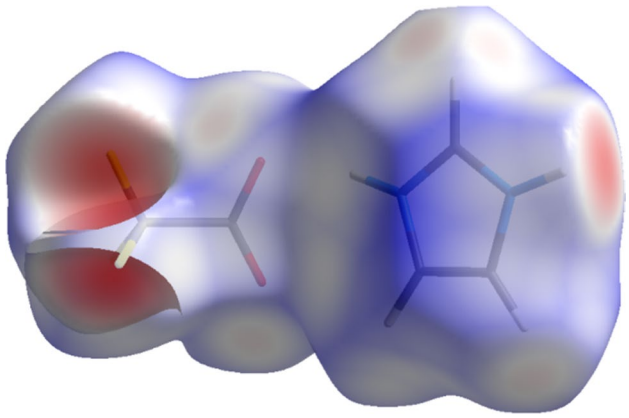

Fig. 8 Hirshfeld surface map of ITF (d norm)

decomposition before the melting point 142 °C confirmed the absence of water molecules in a crystal lattice. From the results it is revealed that ITF crystal is melted before decomposition, so that ITF crystal may useful for optical application up to melting point at 142 °C.

3.7 Hirshfeld surface analysis

The molecular packing arrangements in the crystal and their inter and intramolecular interactions are direct to the distinct material [24, 25]. The Hirshfeld surface analysis is a tool to explore the molecular packing arrangements in crystal, shape and distinct atoms contribution in the crystalline material from 2D fingerprint plots using Crystal Explorer 3.1 program [25, 26]. The surface peculiar colors to signify the intermolecular interaction in which dark red and blue regions indicate that the distance of intermolecular interaction is less than and greater than the Van der Walls distances respectively. Conceivably, the white regions specify the intermolecular distances are equivalent to the Van der Walls distances. In fingerprint plots, di and de denotes as the distance between the Hirshfeld surface to the interior and exterior atom respectively [28]. The ITF Hirshfeld surface map (d norm) is as shown in Fig. 8, the dark-red regions around fluorine atoms revealed the presence of hydrogen bond interaction with the hydrogen atom of NH in imidazolium ring and halogenate bond interactions of fluorine. The trifluoroacetate (anion) highly bind with imidazolium (cation) ring through hydrogen bond interactions (N–H···O) and (C–H···O). The 2D fingerprint plots are as illustrated in Fig. 9. The O···H/H···O (25.2%) and F···H/H···F (23.8%) kinds of hydrogen bond interactions are the most superior factor to decide crystalline packing arrangements of ITF. The intriguing halogen bond F···F interaction is present in the titled compound, and their interaction contribution is 21.7%.

3.8 NLO analysis

The second order NLO activity of the title compound was experimentally confirmed from the Kurtz-Perry technique [29]. The Nd-YAG laser (1064 nm) has the input energy of 1.2 mJ/pulse is used as the input source for characterization. The second harmonic signal confirmed from the 532 nm green emission from the ITF powder sample, and the emission intensity was compared with KDP material. The second harmonic signal of ITF is about 35 mV, and the standard KDP sample holds 21 mV for the same condition.

The quantum chemical calculation is an essential tool to comprehend the origin of microscopic nonlinear activity of the molecules. The delocalized electrons, charge transfer and their accumulations in a molecular crystal are the influential factors to decide the optical activity of the materials. In this work, the finite field approach is used to predict the polarizabilities. The first-order hyperpolarizability has 27 tensor components in the matrix; due to the Kleinman symmetry, it reduced into ten and depicted in Table 5. The total dipole moment, polarizability and first-order polarizability are estimated from the subsequent relations,

$$\mu = \left(\mu_x^2 + \mu_y^2 + \mu_z^2\right)^{1/2}$$

$$\alpha = \frac{1}{3}\left(\alpha_{xx} + \alpha_{yy} + \alpha_{zz}\right)$$

$$\beta = \left(\beta_x^2 + \beta_y^2 + \beta_z^2\right)^{1/2}$$

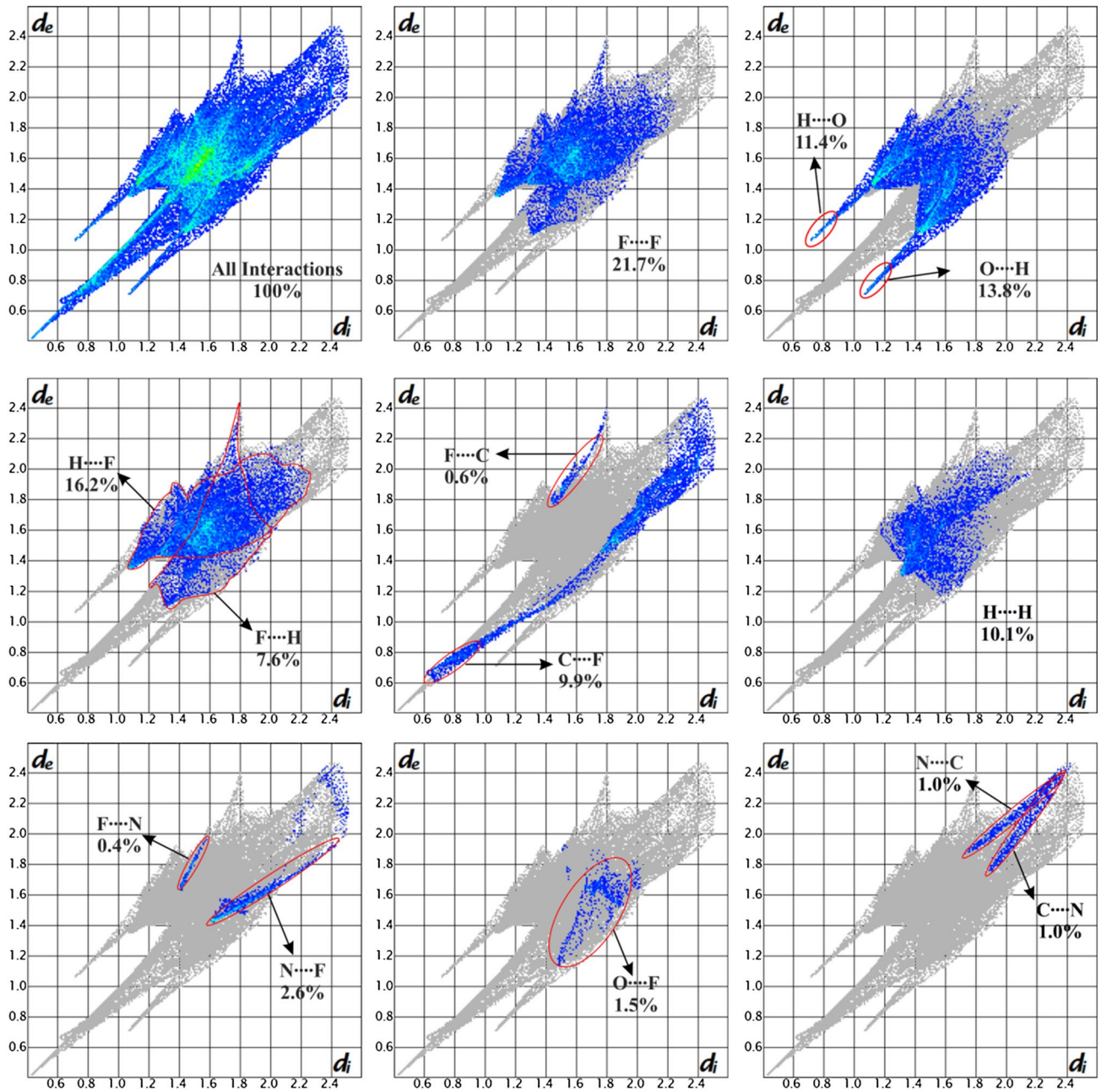

Fig. 9 Fingerprint plots of ITF

Where,

$\beta_x = \beta_{xxx} + \beta_{xxy} + \beta_{xxz}$, $\beta_y = \beta_{yyy} + \beta_{yyz} + \beta_{yyx}$ and $\beta_z = \beta_{zzz} + \beta_{zzx} + \beta_{zzy}$

The total dipole moment, polarizability and first-order hyperpolarizability values are 8.2728 D, −55.7487 esu and 1.0443 esu respectively. From the tensor components amplitude, the charges are mostly accommodated in the X-direction, which was contemplated the dipole moment and first-order hyperpolarizability components. Furthermore, the dipole moment and first order hyperpolarizability values are 6 and 2.8 times that of standard organic molecule urea respectively ($\mu_{urea} = 1.3732$ D and $\beta_{urea} = 0.3728 \times 10^{-30}$ esu) [30]. The nonzero values of β components strongly ensure the higher-order nonlinear activity of the material.

Table 5 The calculated values of dipole moment ($\mu \times 10^{-18}$ esu), polarizability ($\alpha \times 10^{-24}$ esu), and first-order hyperpolarizability ($\beta \times 10^{-30}$ esu) of ITF

Components	Calc. value (a.u)	Calc. value ($\times 10^{-24}$ esu)	Components	Calc. value (a.u)	Calc. value ($\times 10^{-30}$ esu)
μ_x	−8.1644 D	–	β_{xxx}	−136.515	−1.1793
μ_y	−1.335 D	–	β_{xxy}	−17.1035	−0.1477
μ_z	0.0012 D	–	β_{xyy}	−7.0114	−0.0605
μ_{total}	8.2728 D	–	β_{yyy}	−10.1885	−0.0880
α_{xx}	−36.2323	−5.3696	β_{xxz}	0.1195	0.0010
α_{xy}	3.5744	0.5297	β_{xyz}	−0.0514	−0.0004
α_{yy}	−64.173	−9.5104	β_{yyz}	0.2462	0.0021
α_{xz}	−0.0647	−0.00958	β_{xzz}	25.8522	0.2233
α_{zz}	−66.8408	−9.9058	β_{yzz}	−0.3661	−0.0031
α_{yz}	0.049	0.0072	β_{zzz}	−0.1425	−0.0012
α_{total}	−55.7487	−8.2619	β_{total}	120.8811	1.0443 ($=7.61 \times \beta_{Urea}$)

$\beta_{Urea} = 0.137 \times 10^{-30}$ esu

4 Conclusion

Imidazolium trifluoroacetate (ITF) single crystal grown by the slow evaporation method, and double distilled water used as the solvent. The X-ray diffraction patterns effectively confirmed the crystalline structure of ITF. The deprotonation of a carboxyl group and distinctive functional groups existent in the molecule are interpreted from the vibrational analysis. The ITF crystal possesses higher than 60% transmission in the entire visible region, and the optical window is 233–900 nm. The optimized geometrical parameters are very closer to the experimental bond length and bond angles. The intermolecular and intramolecular interactions and their corresponding stabilization energies are derived from NBO analysis in gas phase environment. The decomposition and melting point (142 °C) of the crystal were confirmed from the thermal analysis. The high value of the HOMO–LUMO energy gap reveals that charge transfer is taking place through the intermolecular interaction of N5–H6···O13. Quantitatively and graphically the intermolecular interactions found in the crystal was explored by Hirshfeld surface analysis in a crystalline environment. The second harmonic efficiency of the material is 1.67 times higher than that of typical KDP, and the first-order hyperpolarizability is higher than the organic molecule urea. These experimental and density functional studies manifest that ITF crystal is a proficient material for optoelectronic applications in the visible region.

References

1. D.S. Chemla, J. Zyss, *Nonlinear Optical Properties of Organic Molecules and Crystals*, vol. 1 (Academic Press, Orlando, 1987)
2. D.J. Williams, *Nonlinear Optical Effects in Molecules and Polymers* (Wiley, New York, 1987)
3. L.T. Cheng, W. Tam, S.R. Marder, A.E. Stiegman, G. Rikken, C.W. Spangler, J. Phys. Chem. **95**, 10643 (1991)
4. H.S. Nalwa, Adv. Mater. **5**, 341 (1993)
5. N.J. Long, Angew. Chem. Int. Ed. Engl. **34**, 21 (1995)
6. C. Bosshard, *Organic Nonlinear Optical Materials* (Wiley, Weinheim, 1998)
7. M. hua Jiang, Q. Fang, Adv. Mater. **11**, 1147 (1999)
8. N.E. Heimer, R.E. Del Sesto, Z. Meng, J.S. Wilkes, W.R. Carper, J. Mol. Liq. **124**, 84 (2006)
9. S. Anandhi, T.S. Shyju, T.P. Srinivasan, R. Gopalakrishnan, J. Cryst. Growth **335**, 75 (2011)
10. M. Rajasekar, S. Meenakshisundaram, G. Bhagavannarayana, V. Meenatchi, K. Meena, K. Muthu, Spectrochim. Acta A **124**, 663 (2014)
11. V. Mathivanan, S.G. Raj, G.R. Kumar, T. Raghavalu, R. Mohan, K.S. Kumar, M. Kovendhan, B. Varghese, Main Gr. Chem. **5**, 191 (2006)
12. M.J. Frisch, G.W. Trucks, H.B. Schlegel, G.E. Scuseria, M.A. Robb, J.R. Cheeseman, G. Scalmani, V. Barone, B. Mennucci, G.A. Petersson, H. Nakatsuji, M. Caricato, X. Li, H.P. Hratchian, A.F. Izmaylov, J. Bloino, G. Zheng, J.L. Sonnenberg, M. Hada, M. Ehara, K. Toyota, R. Fukuda, J. Hasegawa, M. Ishida, T. Nakajima, Y. Honda, O. Kitao, H. Nakai, T. Vreven, J.A. Montgomery, J.E. Peralta, F. Ogliaro, M. Bearpark, J.J. Heyd, E. Brothers, K.N. Kudin, V.N. Staroverov, T. Keith, R. Kobayashi, J. Normand, K. Raghavachari, A. Rendell, J.C. Burant, S.S. Iyengar, J. Tomasi, M. Cossi, N. Rega, J.M. Millam, M. Klene, J.E. Knox, J.B. Cross, V. Bakken, C. Adamo, J. Jaramillo, R. Gomperts, R.E. Stratmann, O. Yazyev, A.J. Austin, R. Cammi, C. Pomelli, J.W. Ochterski, R.L. Martin, K. Morokuma, V.G. Zakrzewski, G.A. Voth, P. Salvador, J.J. Dannenberg, S. Dapprich, A.D. Daniels, O. Farkas, J.B. Foresman, J.V. Ortiz, J. Cioslowski, D.J. Fox, *Gaussian, 09 Rev A.02* (Gaussian Inc., Wallingford, 2010)
13. A. Frisch, A.B. Nielson, A.J. Holder, *Gauess View User Manual* (Gaussian Inc, Pittsburgh, 2000)
14. J.D. Patterson, *Density-Functional Theory of Atoms and Molecules* (Oxford University Press, Oxford, 1989)
15. P. Lucaioli, E. Nauha, I. Singh, N. Blagden, Cryst. Growth Des. **18**, 4682 (2018)
16. A. Altomare, C. Giacovazzo, A. Guagliardi, A.G.G. Moliterni, R. Rizzi, P.E. Werner, J. Appl. Crystallogr. **33**, 1180 (2000)
17. E.D. Glendening, R.L. Clark, W. Frank, J. Comput. Chem. **34**, 1429 (2013)

18. R. Srivastava, F.A.M. Al-Omary, A.A. El-Emam, S.K. Pathak, M. Karabacak, V. Narayan, S. Chand, O. Prasad, L. Sinha, J. Mol. Struct. **1137**, 725 (2017)
19. A. Zülfikaroğlu, H. Batı, N. Dege, J. Mol. Struct. **1162**, 125 (2018)
20. R. Anbarasan, J. Kalyana Sundar, M. Anna Lakshmi, J. Mol. Struct. **1179**, 154 (2018)
21. S. Liu, C.K. Schauer, J. Chem. Phys. **142**, 054107 (2015)
22. R. Anbarasan, M. Anna Lakshmi, J. Kalyana Sundar, J. Mater. Sci.: Mater. Electron. **29**, 14827 (2018)
23. J.C. Lorquet, Rev. Mod. Phys. **32**, 312 (1960)
24. M.C. Etter, J. Phys. Chem. **95**, 4601 (1991)
25. M.A. Spackman, D. Jayatilaka, CrystEngComm **11**, 19 (2009)
26. M.J. Turner, J.J. McKinnon, S.K. Wolff, D.J. Grimwood, P.R. Spackman, CrystalExplorer17 (University of Western Australia, 2017)
27. S.K. Wolff, D.J. Grimwood, J.J. McKinnon, M.J. Turner, D. Jayatilaka, M.A. Spackman, *Univ* (West, Aust, 2012)
28. J.J.M.M.A. Spackman, CrystEngComm **4**, 378 (2002)
29. S.K. Kurtz, T.T. Perry, J. Appl. Phys. **39**, 3798 (1968)
30. R. Anbarasan, P. Eniya, M. Anna Lakshmi, J. Kalyana Sundar, J. Mol. Struct. **1188**, 165 (2019)